ADVANCED MATERIALS
www.advmat.de

Interplay of Different Major Ampullate Spidroins during Assembly and Implications for Fiber Mechanics

*Merisa Saric, Lukas Eisoldt, Volker Döring, and Thomas Scheibel**

Major ampullate (MA) spider silk has fascinating mechanical properties combining strength and elasticity. All known natural MA silks contain at least two or more different spidroins; however, it is unknown why and if there is any interplay in the spinning dope. Here, two different spidroins from *Araneus diadematus* are co-produced in *Escherichia coli* to study the possible dimerization and effects thereof on the mechanical properties of fibers. During the production of the two spidroins, a mixture of homo- and heterodimers is formed triggered by the carboxyl-terminal domains. Interestingly, homodimeric species of the individual spidroins self-assemble differently in comparison to heterodimers, and stoichiometric mixtures of homo- and heterodimers yield spidroin networks upon assembly with huge impact on fiber mechanics upon spinning. The obtained results provide the basis for man-made tuning of spinning dopes to yield high-performance fibers.

Spider silk fibers are the toughest known biopolymeric materials in nature combining strength and elasticity.[1] Among all spider silk types, major ampullate (MA) silk, also known as dragline silk, is most intensely studied due to its accessibility through the possibility of silking spiders, which is not as easily possible for other silk types.[2] MA silk threads comprise several proteins, known as major ampullate spidroins (MaSps), which differ among spiders concerning molecular weight, amino acid composition and functional (i.e., mechanical) impact on mechanical properties.[3–6] Most prominent spidroins are MaSp1 and MaSp2, which mainly exhibit differences in their proline content (MaSp 1 < 0.4%, MaSp2 > 10%).[7] In some spiders also short variants of MaSp1 (i.e., MaSp1s) and other MaSp variants such as MaSp3 and MaSp4 have been identified with unknown impact on fiber performance.[4,8–10] Among MA silk that of *Araneus diadematus* has a surprisingly high proline content based on the unusual presence of two MaSp2 variants, named *A. diadematus* fibroin (ADF) 3 and 4, which is a unique attribute among the known orb-weaver spiders.[7] Both ADF proteins are secreted in the same compartment of the spinning gland.[11] Genome analysis suggests that different MaSps are produced within the same cell as opposed to separated cells, which led to the assumption that they might already interact within the cell shortly after translation (e.g., along the secretory pathway).[12,13]

Most MA spidroins comprise a large repetitive core domain, flanked by small non-repetitive terminal domains (TDs) (**Figure 1**a),[3] and the exact composition of MaSps in spider silk fibers depends on the spider species.[14–16] Individual repeats consist of 30–60 amino acid residues with specific amino acid motifs. The most prominent motif in MaSp is a polyalanine stretch of 5–14 residues depending on the spider species.[17] In the final fiber, the polyalanine stretches form tightly packed β-sheet crystallites responsible for its mechanical strength.[18–21] Other common amino acid motifs are GGX or GPGXX, which form loosely structured regions that may contribute to the flexibility of the fiber.[18,22,23] While GGX is found predominantly in MaSp1, GPGXX stretches are mostly found in MaSp2.[7,13] MaSp3 lacks typical poly-alanine or GPG motifs, but exhibits explicitly more polar and acidic residues in comparison to MaSp1 and MaSp2.[4] The silk gene transcript of MaSp4, highly expressed in *Caerostris darwini* spinning glands, contains a unique GPGPQ amino acid motif and might be a quite special variant found in this explicit species.[10]

However, spidroin sequence composition is only one factor important for fiber performance, and other factors, such as environmental, nutrition or stress levels, also play a crucial role.[14–16] Assembly of MaSps is mainly coordinated through their TDs. In contrast to the repetitive core domains with varying sequences, the TDs of MaSps are evolutionary highly conserved.[24,25] Amino- (NTD) and carboxyl-terminal domains (CTD) play a significant role in preventing protein aggregation within the spiders' gland as well as in vitro and control self-assembly of spidroins into highly ordered fibrils and fibers upon external triggers such as ion exchange, acidification and shear force.[26] In general, it could be shown that TDs play a significant role in the formation of supramolecular, micellar-like assemblies important for storage of the spidroins at high concentrations in the spinning dope, as well as in alignment of recombinant MaSps during fiber assembly.[27–34] The conversion of the liquid spinning dope into a solid fiber is enabled within the spinning duct. Amino-terminal MaSp domains remain monomeric at neutral pH and form antiparallel dimers upon acidification.[27,35–37] CTDs of ADF3 and ADF4 comprise five-helix bundles and form disulfide-linked permanent parallel dimers

M. Saric, Dr. L. Eisoldt, V. Döring, Prof. T. Scheibel
Lehrstuhl Biomaterialien
Universität Bayreuth
Prof-Rüdiger-Bormann-Str. 1, Bayreuth 95447, Germany
E-mail: thomas.scheibel@bm.uni-bayreuth.de

The ORCID identification number(s) for the author(s) of this article can be found under https://doi.org/10.1002/adma.202006499.

DOI: 10.1002/adma.202006499

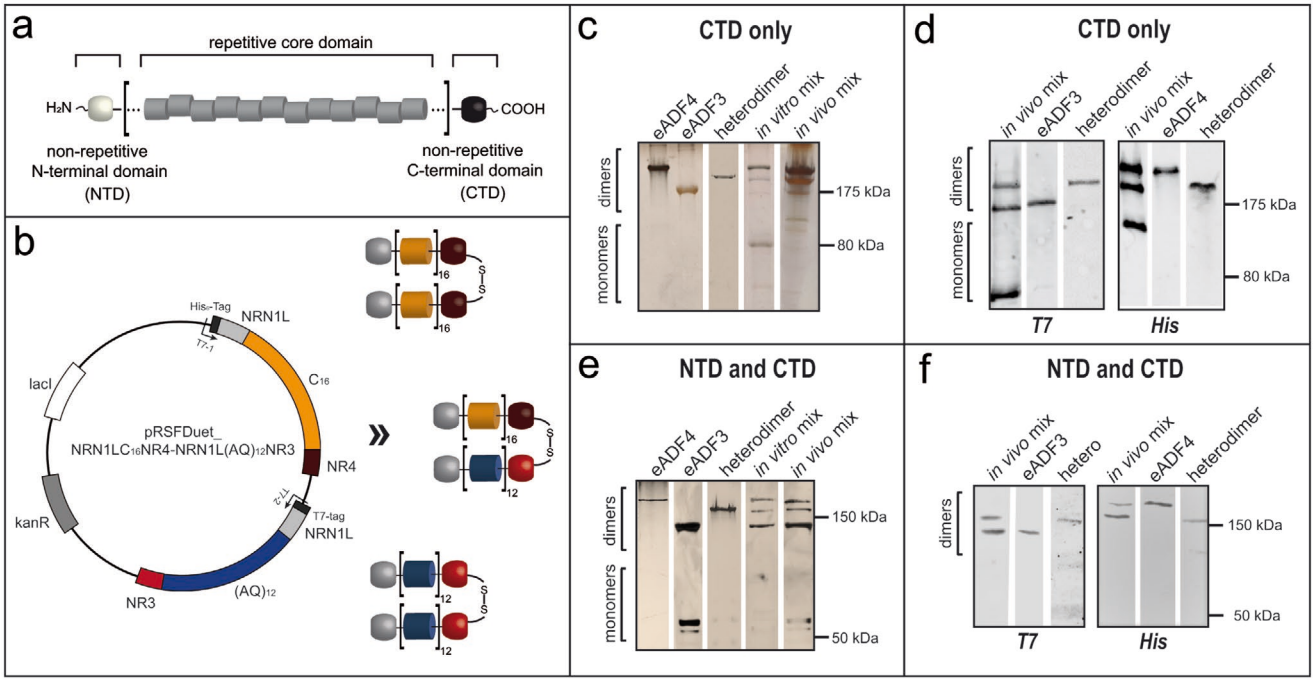

Figure 1. Scheme of used recombinant spider silk proteins and their dimerization state. a) The primary structure of spidroins comprises a highly repetitive core domain flanked by NTDs and CTDs.[3] b) Illustration of the plasmid used for co-expression of engineered genes. An overview of all investigated recombinant proteins derived from ADF3 and ADF4 is given in Figure S2 in the Supporting Information. Details on protein purities are shown in Figures S3 and S4 and Table S1 in the Supporting Information. c–f) Analyses of dimer formation of different ADF variants produced in vitro and in vivo using silver-stained SDS-PAGE (c,e) and western blots (d,f) of purified eADF3-CTD/eADF4-CTD homo- and heterodimers (c,d) and NTD-eADF3-CTD/NTD-eADF4-CTD homo- and heterodimers (e,f). In vivo and in vitro mix samples both contained the mixture of eADF3 (T7-tagged) and eADF4 (His-tagged) variants.

(Figure S1a,b, Supporting Information).[27] Intramolecular salt bridges, based on charged acidic residues and a single arginine, have been shown to be essential for the structural integrity of the tightly folded CTDs.[26] Upon spinning, the CTDs are destabilized by acidification-induced protonation of the acidic side chains. In addition, salting-out and shear forces expose hydrophobic patches on the surfaces of the CTDs, which are anchor points for guiding the correct spidroin alignment along fiber formation.[27]

ADF3 and ADF4 are both MaSp2-type proteins but they exhibit differences in hydropathicity,[38] which has raised the question why *A. diadematus* has two MaSp2 derivatives. Although the molecular nature of individual MaSps is well described, not much is known about the interplay of MaSps and concerning its impact on mechanical properties of spider silk fibers. In this study, we investigated how spidroins of *A. diadematus* interact through their CTDs and how this interaction contributes to self-assembly and fiber mechanics. The amino-terminal domains of *A. diadematus* spidroins have not been identified so far, but NTDs are well conserved throughout MaSps in different spider species as described in detail elsewhere.[25,35] Therefore, the established MaSp1 NTD domain of *Latrodectus hesperus* (Figure S1c,d, Supporting Information) was used to engineer all-domains-containing recombinant proteins.[39,40] Upon co-production in bacteria (in vivo) or refolding (in vitro), the impact of MaSp interplay was investigated on self-assembly in the spinning dope as well as on fiber mechanics upon spinning.

Although ADF3 and ADF4 are both MaSp2-like proteins based on their proline content, they differ significantly in the further sequence of their repetitive core domains yielding quite different hydrophobicity/hydrophilicity.[38] Based on consensus sequences, engineered variants have been designed, produced and purified, varying in the presence/absence of TDs (Figures S2–S4 and Table S1, Supporting Information). Previously, we identified that due to the redox potential of the individual cysteine residues in the CTDs, disulfide-linked dimers were formed even in the cytoplasm of *Escherichia coli*.[27] Since both CTDs of ADF3 and ADF4 show a sequence identity of 58% and a similarity of 73%,[38] we investigated their ability to heterodimerize when incorporated in respective engineered variants (eADF3/4). To analyze effects upon co-expression, *eADF3* and *eADF4* were both cloned into one plasmid under the control of two separate T7-promoters (Figure 1b). To distinguish between both proteins, eADF3 was tagged with an amino-terminal T7 sequence, whereas eADF4 was fused with a hexahistidine (His_6)-tag. eADF3 and eADF4 disulfide-linked dimers were identified upon production in *E. coli* as expected and identified using non-reducing SDS-PAGE followed by western blot analysis, which also showed the presence of heterodimers (Figure 1c–f).

Heterodimerization was also investigated in vitro. Tris(2-carboxyethyl) phosphine was added as a reducing agent to a 1:1 mixture of purified and chemically denatured (with guanidinium thiocyanate) eADF3 and eADF4, followed by refolding in Tris-buffer. Again, SDS-PAGE and western blot analysis revealed the presence of the heterodimer. Interestingly, dimerization took place in a nearly statistical distribution of 1:1:1 of the three dimeric species, two homo- and one heterodimer (Figure 1d,f).

It has been previously shown that the CTDs play an important role in solubilizing spidroins, but also in triggering fiber assembly.[27] TDs respond individually to external stimuli and independently control the core domains' self-assembly process. At physiological pH, the conformational state of dimerized CTDs (with parallel orientation) prevents fiber formation. Upon acidification they switch their conformational state to transform from the soluble into an aligned state which is a prerequisite for fiber assembly.[27] NTDs are monomeric at neutral pH and function as further solubility-enhancing components for the assembly-prone core domain. Upon acidification, NTDs dimerize in an anti-parallel fashion.[35] In order to investigate the impact of C-terminal heterodimerization on self-assembly as a first step, a simplified experimental approach with non-dynamic conditions was needed, and, therefore, only eADFs comprising CTDs were analyzed to begin with. First, isolated heterodimers were compared to each respective eADF3-CTD and eADF4-CTD homodimer, exhibiting hybrid characteristics of both MaSp2 species at the molecular level. Concerning secondary structure content, far-UV-CD indicated no significant differences between the individual protein species (**Figure 2**a). The broad minimum at 205 nm and a plateau at 219 nm indicated a mainly random-coil/PPI-II dominated structure with α-helical portions. The random coil signals arise from the intrinsically unfolded repetitive core domain in solution,[38] whereas the α-helical contributions derive from the nonrepetitive CTDs NR3 and NR4 comprising five helix-bundles.[27,38] Thermal unfolding experiments showed a melting point of 66 °C for the heterodimer, which is 2 °C above that of the eADF3-CTD homodimer and 1.5 °C below that of the eADF4-CTD dimer (Figure 2b). Upon cooling, the heterodimer refolded to the same state as both homodimers, indicating that the process was fully reversible.[38]

Next, self-assembly kinetics of the three dimeric species was analyzed in the presence of phosphate ions (Figure 2c). As shown previously, eADF3 and eADF4 proteins have different assembly and solubility properties, based on the sequence differences of their core domains, when exposed to naturally occurring assembly triggers like phosphate ions or elongational forces.[38,41] eADF4 is known to be more hydrophobic, favorably interacting with other protein molecules and thus aggregating at high concentrations. In contrast, eADF3 appears to be more hydrophilic, as it bonds water molecules and remains fully soluble and conformationally extended at many conditions. These findings could be confirmed, as eADF3-CTD showed the slowest and eADF4-CTD the fastest assembly kinetics under identical conditions. Interestingly, the kinetics of heterodimers was only slightly slower than that of eADF4-CTD homodimers, indicating a strong influence of eADF4 on heterodimer assembly. Since eADF4 has already been shown to self-assemble into cross β-sheet rich fibrils,[42] all three spidroin variants were assembled in the presence of the β-sheet sensitive dye Thioflavin T (ThT) in order to indicate the formation of cross-β-sheet structures (Figure 2d). Throughout the experiment, eADF3 showed significantly (5–10 times) less ThT specific fluorescence than the other two dimeric species, thereby supporting the kinetics results. The self-assembled spidroin variants formed disordered aggregates without any defined structures in case of eADF3-CTD using atomic force microscopy (AFM), eADF4-CTD samples, on the other hand, were clustered, unbranched nanofibrils with varying sizes (Figure 2e,f,h,i). Interestingly, the heterodimers formed also nanofibrils, which were clearly distinctive in form and shape from the respective homodimeric assemblies, revealing a network of short, often branched fibrils sometimes covered by larger filaments (Figure 2g,j). Overall, the heterodimers demonstrated physico-chemical properties derived from both individual proteins.

The AFM results could be confirmed using transmission electron microscopy (TEM) (Figure S5, Supporting Information). TEM was further used to demonstrate how recombinant eADF spidroins assemble in presence or absence of TDs. In case of eADF3, only amorphous aggregates rather than distinct fibrils could be detected, no matter whether terminal domains were present or not (Figure S5a–c, Supporting Information). eADF4 without terminal domains self-assembled into β-sheet-rich nanofibrils as published previously (Figure S5f, Supporting Information).[42] In comparison, eADF4-CTD showed various morphologies of nanofibril-like structures assembled in bundles as well as small aggregates (Figure S5e, Supporting Information), whereas NTD-eADF4-CTD displayed often rather short agglutinated fibril fragments (Figure S5d, Supporting Information). The results indicate that TDs significantly affected the self-assembly process (Figure S5d–f, Supporting Information). Individual heterodimers with CTD or with both NTD and CTD assembled into fibrillary network structures (Figure S5g,h, Supporting Information). Constructs containing mixtures of eADF3 and eADF4 (comprising only CTDs or both TDs) resulted in aggregated assemblies without any fibrillary morphologies (Figure S5i–l, Supporting Information). These results supported the hypothesis that TDs are significantly involved in the control of solubility as well as self-assembly of the spidroin core domains by stabilizing the soluble state of spidroins.[27]

To investigate the influence of heterodimerization on fiber assembly and fiber mechanics, all-domain NTD-eADF3-CTD and NTD-eADF4-CTD were dimerized upon co-production in *E. coli* or upon refolding in vitro yielding the same stoichiometric ratio of homo- and heterodimers. Aqueous, highly concentrated spinning dopes of the mixtures were prepared akin to a previously published protocol by Heidebrecht et al.[43] Classical spinning dopes (CSD) were achieved using dialysis against poly(ethylene glycol) (PEG) in order to remove water and to obtain high protein concentrations. In contrast, biomimetic spinning dopes (BSD) were processed using dialysis against a phosphate buffer initiating self-assembly of the spidroins yielding a high-density phase.[31] Protein concentrations typically ranged from 10 to 15% w/v. Microfibers were produced using a microfluidic multichannel device[44] to facilitate processing (Figure S6, Supporting Information). Phosphate-containing spinning buffers (30×10^{-3} M potassium phosphate, pH 8) and coagulation baths (0.5–1 M potassium phosphate, pH 6) were employed mimicking the natural spinning environment. Overall, the here presented approach is mimicking parts of the natural assembly process. Based on aqueous highly concentrated spinning dopes, the spidroins were exposed to shear forces on their way from the syringe to the microfluidic chip and further pre-assembled upon addition of low concentrations of phosphate. As soon as the spidroins were extruded into the coagulation bath containing high phosphate concentration at

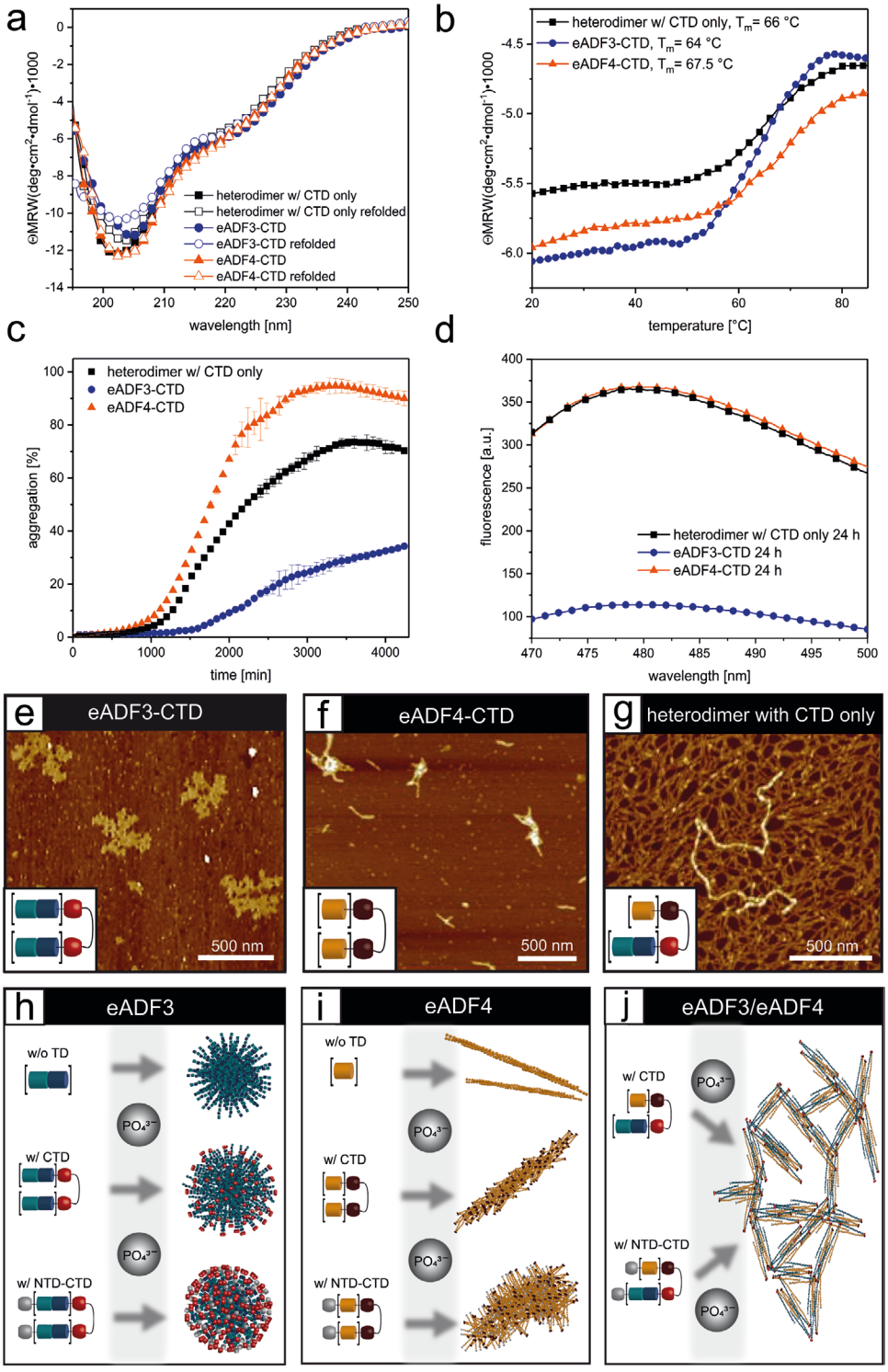

Figure 2. Structural characterization and fibril assembly of individual homo- and heterodimeric spidroins comprising ADF3/4 CTD. a) Far UV circular dichroism spectra of dimeric eADF3-CTD (blue), eADF4-CTD (orange), and the heterodimer consisting of both proteins (black) in Tris-buffer (pH 8). b) Melting points of all three dimer species as determined using far-UV spectroscopy. c) Fibril assembly kinetics of the three dimer species in presence of phosphate buffer (pH 8) by measuring turbidity at 340 nm. d) Thioflavin T binding to fibers made of the dimer species depicted the presence of cross β-sheet-rich structures in the eADF4-containing samples. e–g) Morphologies of assemblies of the dimer species: e) eADF3-CTD, f) eADF4-CTD, and g) eADF3/eADF4-CTD heterodimer in presence of phosphate buffer, investigated using AFM. h–j) Model of self-assembly of the two known MaSp2 variants of *A. diadematus* individually and in a mixture. h) eADF3 preferentially forms large globular-shaped assemblies with little distinct secondary structural elements,[31] whether TDs are present or not. i) eADF4 forms β-sheet-rich nanofibrils,[42] and TDs severely influence nanofibril formation. j) Upon heterodimerization of eADF3-CTD/eADF4-CTD or NTD-eADF4-CTD/NTD-eADF4-CTD, fibrillary network structures could be detected. TD: terminal domain.

Table 1. Comparison of mechanical properties of man-made and natural spider silk fibers. Fibers made of different variants comprising terminal domains were spun in a biomimetic set-up using: a) "classical" spinning dopes 10–13% w/v or b) "biomimetic" self-assembled spinning dopes 15% w/v, poststretched and post-treated. Tensile testing was performed at 30% rH.

a. Classical spinning dope (CSD)

Protein	NTD-eADF3-CTD[a)]	NTD-eADF4-CTD	In vitro mixture with NTD and CTD	In vivo mixture with NTD and CTD	Homodimer blend with NTD and CTD[a)]
Stretching [%]	600	300	350	400	300
Diameter [µm]	31 ± 0.5	29 ± 0.2	36 ± 0.5	29 ± 0.8	32 ± 3
Extensibility [%]	59 ± 1	8 ± 0.2	17 ± 0.9	25 ± 1	17 ± 5
Strength [MPa]	239 ± 12	417 ± 15	308 ± 13	353 ± 14	103 ± 21
Toughness [MJ m^{-3}]	71 ± 3	17 ± 1	26 ± 1	47 ± 2	11 ± 4
Youngs's Modulus [GPa]	1 ± 0.1	4 ± 0.4	2 ± 0.1	3 ± 0.2	1 ± 0.6
Number of samples	$n = 6$	$n = 7$	$n = 7$	$n = 9$	9

b. Biomimetic spinning dope (BSD)

Protein	NTD-eADF3-CTD[a)]	NTD-eADF4-CTD	In vitro mixture with NTD and CTD	In vivo mixture with NTD and CTD	Supercontracted natural MA silk *A. diadematus*
Stretching [%]	600	300	350	400	/
Diameter [µm]	23 ± 1	33 ± 0.3	37 ± 0.4	27 ± 1	5 ± 0.1
Extensibility [%]	80 ± 1	10 ± 0.2	22 ± 0.5	32 ± 1	39 ± 1
Strength [MPa]	329 ± 11	602 ± 26	614 ± 29	834 ± 34	795 ± 42
Toughness [MJ m^{-3}]	137 ± 6	32 ± 2	70 ± 6	143 ± 6	129 ± 6
Youngs's Modulus [GPa]	3 ± 0.3	6 ± 0.5	4 ± 0.2	5 ± 0.4	4 ± 0.2
Number of samples	$n = 7$	$n = 7$	$n = 7$	$n = 7$	$n = 9$

[a)]Fibers produced in a coagulation bath comprising 80% isopropyl alcohol.

low pH, a fiber was formed. In this experimental setup, fibers made from BSD were more homogenous in comparison to those from CSD. Phosphate-induced self-assembly of recombinant spidroins in BSDs obtained fibers with mechanical properties equaling that of a natural fiber (**Table 1**, **Figure 3**). Light microscopy and scanning electron microscopy (SEM) images of all fibers produced demonstrated similar morphological features (Figures S7a–c, S8a–c, BSD, Supporting Information) in case of CSD fibers, only NTD-eADF4-CTD encountered few interior defects (Figures S7a, S8a, CSD, Supporting Information). Tensile properties of all artificially spun fibers were compared to supercontracted (sc) natural MA silk of *A. diadematus*. Supercontracted fibers were used, as natural dragline silks are subjected to a high variability depending on for example spider age and fitness, the temperature and the silking conditions.[45] Supercontraction of forcibly silked fibers is a widely used method, as it yields consistent data and is representative of the real mechanical properties of naturally spun fibers.[46] No solid NTD-eADF3-CTD fibers could be obtained using the microfluidics set-up. Intermolecular interactions of the hydrophilic eADF3 core domain likely impeded proper self-assembly in presence of phosphate and induced rather unspecific agglomeration than fiber assembly. Therefore, NTD-eADF3-CTD fibers were produced in a coagulation bath filled with 80% isopropyl alcohol as described previously.[43] Mechanical properties of fibers derived from BSD comprising the in vivo mixture were comparable to those of natural MA silk concerning all mechanical aspects, such as strength (834 ± 34 MPa), toughness (143 ± 6 MJ m^{-3}) and extensibility (32 ± 1%). As expected, tensile tests of all BSD variants demonstrated considerably improved mechanical properties compared to the corresponding CSD variants. Although not comparable to the in vivo mixture, the mechanical characteristics of in vitro BSD fibers outperformed those from one-protein fibers, being twice as extensible (22 ± 0.5%) compared to NTD-eADF4-CTD and twice as strong (614 ± 29 MPa) compared to NTD-eADF3-CTD fibers (Table 1b, Figure 3). Fibers spun from NTD-eADF4-CTD (BSD and CSD) could be poststretched only up to 300% and displayed lower values for tensile strength, toughness, and extensibility compared to the other variants, but the highest Young's Modulus (6 ± 0.5 MPa) of all tested artificial fiber samples. The mechanical differences between in vitro and in vivo fibers might be due to spidroin folding. During in vivo co-production in *E. coli*, the cellular chaperon machinery ensures efficient protein folding. Molecular chaperones interact co-translationally with the nascent polypeptide chain emerging from ribosomes, minimizing the probability of premature misfolding.[47,48] The in vivo protein mixture was purified to yield properly folded proteins with "native-like" conformations. In the course of producing in vitro mixtures, individual homodimers had to be chemically denatured and reduced first, before refolding and dimerization took place in step-wise dialysis by gradually removing the denaturant from the proteins. During this procedure, spidroins may have partially folded into intermediate or misfolded states.[49] The fact that poststretching of in vitro fibers was possible up to 350% of the initial length without breaking compared to in vivo ones (poststretching up to 400%) underlines that spidroin assembly probably was impeded by present misfolded proteins

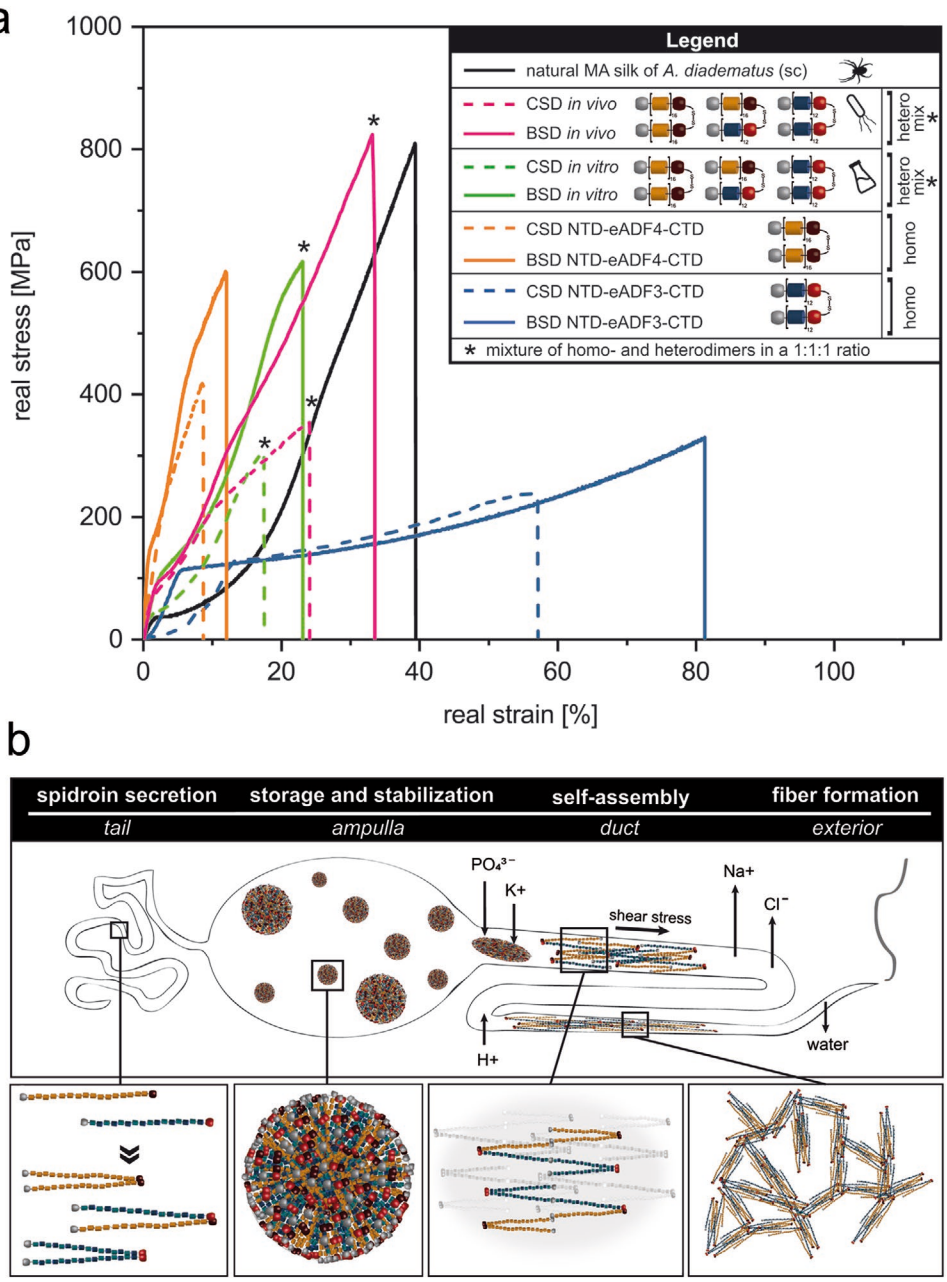

Figure 3. Real stress–strain curves of recombinant and natural spider silk fibers. a) Tensile tests of poststretched fibers of eADF3 and eADF4 spun from classical (CSD, colored dashed lines) as well as biomimetic (BSD, colored solid lines) spinning dopes were made in comparison to those of sc natural *A. diadematus* major ampullate spidroin fibers (black). Mechanical properties of fibers are displayed spun of eADF3/eADF4 homo- and heterodimers mixtures from in vivo production in *E. coli* (pink) and in vitro production (green), as well as one-protein fibers composed of NTD-eADF4-CTD (orange) or NTD-eADF3-CTD (blue). b) Upon co-production, spidroins form both homo- and heterodimers. In the course of assembly, micellar-like structures have been identified which formed by microphase separation.[31,33,34,36] In the spinning duct, factors such as ion exchange, acidification and shear stress initiate fiber assembly of the spinning dope.[32] A mixture of homo- and heterodimers of eADF3 and eADF4 yield highly interconnected networks of the differently structured proteins, which allow the production of fibers with significantly improved mechanical properties due to a better load dissipation based on the combination of crystallinity (eADF4) and elasticity (eADF3).

in the in vitro dopes, causing slightly less structural alignment of the molecules within the fiber yielding lower mechanical properties (Table 1b, Figure 3).

Additionally, blends containing the two homodimers (NTD-eADF3-CTD and NTD-eADF4-CTD) were tested (Table 1; Figure S9, Supporting Information). Interestingly, no BSD could be obtained with this mixture due to aggregation during phosphate dialysis. Since eADF3 and eADF4 exhibit different assembly behaviors, the behaviors of the respective homodimers probably interfered during assembly. Although CSDs could be obtained, fibers could only be produced in an isopropyl alcohol coagulation setup similar to NTD-eADF3-CTD fibers.

The overall mechanical properties of homodimer blend fibers were much lower (Table 1) than that of CSD and BSD fibers spun from mixtures additionally containing the heterodimer. Consequently, the presence of the heterodimer and assemblies made thereof likely serves as a mediator between individual eADF3 assemblies and eADF4 assemblies within the dope and during fiber formation. It is supposed that the assemblies of the respective homodimers are integrated in an interpenetrating network derived from the heterodimers, significantly enhancing the mechanical characteristics of fibers. Therefore, fibers spun from in vivo mixtures combined mechanical features of each component with NTD-eADF4-CTD contributing to strength and NTD-eADF3-CTD to extensibility of the fibers.

Mimicking natural spider silk fibers has been a challenging task, as despite decades of research it has not yet been possible to imitate its' hierarchical structure and its mechanical properties. Especially it is of particular importance to stay as close to the natural process as possible (i.e., being biomimetic) to obtain hierarchically structured fibers with mechanical properties equaling that of natural ones. Inspired by the complex natural spinning process from the molecular to the macroscopic level, our approach sheds light on the underlying molecular mechanisms important for proper assembly. The two known MaSp2 derivatives of *A. diadematus*, ADF3 and ADF4, exhibit different physicochemical characteristics. While the recombinant variant eADF3 assembles without significant β-sheet content and the assemblies show micellar-like appearance (Figure 2h),[31] recombinant eADF4 can assemble into nanosized cross-β-fibrils (Figure 2i). [42] Intriguingly, heterodimerization initiated by the CTDs of these spidroins gained fibrillary network structures upon assembly (Figure 2j). Utilizing these molecular features in combination with biomimetic spinning yielded mechanically nature-like performing fibers. Our findings support the hypothesis that intermolecular interactions of TDs in the spinning dope control structural alignment as well as formation of higher-order protein structures (Figure 3b).[36,50] Ultimately, this work underlines the importance of MaSp interaction at a (supra)molecular level and the contribution of this interplay to control solubility as well as self-assembly with significant impact on the mechanical performance of fibers.

In a biological context, spiders can regulate the expression of spider silk genes and subsequently control protein content with obvious implications on assembly properties. This comes in line with the finding that spiders tune or adapt their fiber mechanics, which is an important attribute when spiders are exposed to fluctuating environmental conditions.[51] Our findings will allow to develop man-made high-performance bioinspired fibers, in which the combination of proteins will utilize functional complexity and opens up new expedient properties useful for a whole set of novel applications.

Experimental Section

Protein Production: The individually produced proteins eADF3-CTD ($(AQ)_{12}$NR3), NTD-eADF3-CTD (NRN1L$(AQ)_{12}$NR3), eADF4-CTD (C_{16}NR4) and NTD-eADF4-CTD (NRN1LC_{16}NR4) bearing N-terminal T7-tags were produced and purified as described previously.[38,41] For co-expression, genes encoding eADF3-CTD/NTD-eADF3-CTD (T7-Tag) and eADF4-CTD/NTD-eADF4-CTD (His-Tag) were cloned into a pRSFDuet-1 expression vector bearing two multiple cloning sites. Gene expression and protein purification was carried out similar to the previously published procedure.[38] The CTD heterodimer was purified using an immobilized metal ion affinity chromatography (HisTrap HP, GE Healthcare), followed by an anion exchange column (Q Sepharose FF, GE Healthcare).

Protein Preparation and Analysis: Lyophilized proteins were dissolved in 6 M guanidinium thiocyanate and dialyzed three times against 50×10^{-3} M Tris/HCl pH 8, 150×10^{-3} M NaCl at room temperature (RT). Protein aggregates were separated upon centrifugation at 130 000 $\times g$ for 20 min at RT. Protein samples were investigated using 8%, 10%, or 12% SDS-PAGE (2.5 µg protein). Gels were either silver stained or used for western blot (WB) analysis. WBs were analyzed using His-Tag or T7-Tag antibody HRP conjugates (Novagen) and ECL plus (GE Healthcare) according to the manufacturers' recommendations. For circular dichroism spectroscopy measurements, proteins were dialyzed against 10×10^{-3} M Tris-buffer buffer (pH 8), centrifuged at 180 000 $\times g$ for 1 h at 4 °C and diluted to 3.4×10^{-6} M. Far-UV circular dichroism spectra were recorded (Jasco J-715) in triplicates using cuvettes with 0.1 cm path lengths and spectra were subsequently smoothed by applying a Savitzky–Golay filter. Thermal transitions were determined recording changes at 220 nm with heating/cooling rates of 1 °C min^{-1}.

Self-Assembly Analyzes: Fibril formation of the different protein variants was triggered at similar conditions as described previously.[52] Proteins were dialyzed against 10×10^{-3} M Tris/HCl, pH 8 and ultracentrifuged at 180 000 $\times g$ for 1 h at 4 °C. Assembly was started upon addition of sodium phosphate or potassium phosphate (pH 8) at a final concentration of $50–100 \times 10^{-3}$ M at 20 °C. Turbidity assays were recorded at 340 nm in triplicates using UV/vis spectrometry. For assembly kinetics, 10×10^{-6} M ThT was added to proteins dissolved in phosphate buffer and transferred to Quartz UV-microcuvettes. The fluorescence was monitored at an excitation wavelength of 440 nm after 24 h of incubation at 25 °C. Assembly morphologies were analyzed using TEM or AFM. A transmission electron microscope (JEOL JEM-2100) was used, and images were taken using a device camera (UltraScan 4000, Gatan Inc.) with Gatan Digital Micrograph software. AFM scanning (Dimension ICON, NanoScope V controller, Bruker) was performed in TappingMode using Si cantilevers (OTESPA-R3, f_0 300 kHz, k: 26 N m^{-1}, Bruker). Data processing was done using NanoScope Analysis software 1.5 (Bruker).

Production and Analyzes of Fibers: Spinning dopes were prepared as previously described.[43] Lyophilized proteins were dissolved in 6 M guanidinium thiocyanate and dialyzed against 50×10^{-3} M Tris/HCl, pH 8.0, 150×10^{-3} M NaCl. CSD were prepared upon dialysis against a 20% w/v PEG (35 kDa) solution, and BSD were obtained by dialysis against 30×10^{-3} M potassium phosphate buffer (pH 8). For fiber production, spinning dopes were extruded at flow rates of 50–150 µL h^{-1} through a microfluidic chip into a coagulation bath filled with 0.5–1 M potassium phosphate buffer (pH 6). 30×10^{-3} M potassium phosphate buffer (pH 8) was used as sheath flows at 600–800 µL h^{-1}. Only fibers spun from NTD-eADF3-CTD were produced using a different coagulation bath comprising 80% isopropyl alcohol as described previously.[43] All fibers were manually poststretched to maximum in 80% isopropyl alcohol, post-treated in 70% ethanol, and analyzed using an optical microscope (Leica DMI3000B, software Leica V4.3). Fiber diameters were monitored with 20×, 40×, and 100× object lenses. From each fiber sample, several representative images were analyzed at different sites ($n \geq 10$) to measure the quadratic mean of the fiber diameter and its standard deviation. For SEM, fiber samples were sputter-coated with 1.3 nm platinum (EM ACE600 sputter coater, Leica) and imaged (Apreo VS, Thermo Fisher Scientific). For tensile testing, fiber sections ($n \geq 7$) were placed on plastic sample holders with a 2 mm gap using superglue (UHU GmbH Co. KG). Female, adult *A. diadematus* spiders were fed with fruit flies; fibers were collected by forcibly silking at 12 cm s^{-1}, and submerged into distilled water for supercontraction. Tensile testing (BOSE Electroforce 3220) was performed using a 0.49 N load cell at a pulling rate of 0.005 mm s^{-1} at 30% relative humidity. Mechanical properties were quantitatively evaluated using Microsoft Excel 2016

(Microsoft Corporation, Redmond, WA, USA) or Origin 9.4 (OriginLab Corporation, Northhampton, MA, USA) considering real stress and real strain data.

Supporting Information

Supporting Information is available from the Wiley Online Library or from the author.

Acknowledgements

The authors thank Anika Winkler for TEM imaging, and Claudia Stemmann as well as Dr. Hendrik Bargel for SEM measurements. Further, the authors would like to thank Svenja Schiemann for kinetic assembly measurements, and Yeldem Koc for assistance in cloning of spidroin variants. The authors thank Dr. Elise Liensdorf and Dr. Stephen Strassburg for proof reading. Financial support was provided by the Deutsche Forschungsgemeinschaft SFB 840 TP A08.

Open access funding enabled and organized by Projekt DEAL.

Conflict of Interest

T.S. is co-founder and shareholder of the company AMSilk GmbH.

Data Availability Statement

Research data are not shared.

Keywords

bioinspired fibers, heterodimers, protein interplay, self-assembly, spider silk

Received: September 23, 2020
Revised: December 17, 2020
Published online:

[1] F. Vollrath, *Rev. Mol. Biotechnol.* **2000**, *74*, 67.
[2] M. Heim, D. Keerl, T. Scheibel, *Angew. Chem., Int. Ed.* **2009**, *48*, 3584.
[3] M. Xu, R. V. Lewis, *Proc. Natl. Acad. Sci. USA* **1990**, *87*, 7120.
[4] M. A. Collin, T. H. Clarke III, N. A. Ayoub, C. Y. Hayashi, *Int. J. Biol. Macromol.* **2018**, *113*, 829.
[5] L. Han, L. Zhang, T. Zhao, Y. Wang, M. Nakagaki, *Int. J. Biol. Macromol.* **2013**, *56*, 156.
[6] S. M. Correa-Garhwal, T. H. Clarke, M. Janssen, L. Crevecoeur, B. N. McQuillan, A. H. Simpson, C. J. Vink, C. Y. Hayashi, *Sci. Rep.* **2019**, *9*, 13656.
[7] P. A. Guerette, D. G. Ginzinger, B. H. Weber, J. M. Gosline, *Science* **1996**, *272*, 112.
[8] N. Kono, H. Nakamura, R. Ohtoshi, D. A. P. Moran, A. Shinohara, Y. Yoshida, M. Fujiwara, M. Mori, M. Tomita, K. Arakawa, *Sci. Rep.* **2019**, *9*, 8380.
[9] C. Thamm, T. Scheibel, *Biomacromolecules* **2017**, *18*, 1365.
[10] J. E. Garb, R. A. Haney, E. E. Schwager, M. Gregorič, M. Kuntner, I. Agnarsson, T. A. Blackledge, *Commun. Biol.* **2019**, *2*, 275.
[11] F. Vollrath, D. P. Knight, *Nature* **2001**, *410*, 541.
[12] W. A. Gaines IV, W. R. Marcotte Jr., *Insect Mol. Biol.* **2008**, *17*, 465.
[13] N. A. Ayoub, J. E. Garb, R. M. Tinghitella, M. A. Collin, C. Y. Hayashi, *PLoS One* **2007**, *2*, e514.
[14] S. J. Blamires, C.-L. Wu, I.-M. Tso, *PLoS One* **2012**, *7*, e31626.
[15] K. H. Guehrs, B. Schlott, F. Grosse, K. Weisshart, *Insect Mol. Biol.* **2008**, *17*, 553.
[16] D. B. Zax, D. E. Armanios, S. Horak, C. Malowniak, Z. Yang, *Biomacromolecules* **2004**, *5*, 732.
[17] X. Hu, K. Vasanthavada, K. Kohler, S. McNary, A. Moore, C. Vierra, *Cell. Mol. Life Sci.* **1986**, *63*, 2006.
[18] J. D. Van Beek, S. Hess, F. Vollrath, B. Meier, *Proc. Natl Acad. Sci. USA* **2002**, *99*, 10266.
[19] A. D. Parkhe, S. K. Seeley, K. Gardner, L. Thompson, R. V. Lewis, *J. Mol. Recognit.* **1997**, *10*, 1.
[20] D. H. Hijirida, K. G. Do, C. Michal, S. Wong, D. Zax, L. W. Jelinski, *Biophys. J.* **1996**, *71*, 3442.
[21] A. Simmons, E. Ray, L. W. Jelinski, *Macromolecules* **1994**, *27*, 5235.
[22] T. Lefevre, J. Leclerc, J.-F. Rioux-Dubé, T. Buffeteau, M.-C. Paquin, M.-E. Rousseau, I. Cloutier, M. Auger, S. M. Gagné, S. Boudreault, *Biomacromolecules* **2007**, *8*, 2342.
[23] A. H. Simmons, C. A. Michal, L. W. Jelinski, *Science* **1996**, *271*, 84.
[24] R. Challis, S. Goodacre, G. Hewitt, *Insect Mol. Biol.* **2006**, *15*, 45.
[25] J. E. Garb, N. A. Ayoub, C. Y. Hayashi, *BMC Evol. Biol.* **2010**, *10*, 243.
[26] J. Bauer, T. Scheibel, *Biomacromolecules* **2017**, *18*, 835.
[27] F. Hagn, L. Eisoldt, J. G. Hardy, C. Vendrely, M. Coles, T. Scheibel, H. Kessler, *Nature* **2010**, *465*, 239.
[28] L. Eisoldt, J. G. Hardy, M. Heim, T. R. Scheibel, *J. Struct. Biol.* **2010**, *170*, 413.
[29] M. Stark, S. Grip, A. Rising, M. Hedhammar, W. Engström, G. Hjälm, J. Johansson, *Biomacromolecules* **2007**, *8*, 1695.
[30] A. Sponner, W. Vater, W. Rommerskirch, F. Vollrath, E. Unger, F. Grosse, K. Weisshart, *Biochem. Biophys. Res. Commun.* **2005**, *338*, 897.
[31] J. H. Exler, D. Hümmerich, T. Scheibel, *Angew. Chem., Int. Ed.* **2007**, *46*, 3559.
[32] L. Eisoldt, T. Scheibel, A. Smith, *Mater. Today* **2011**, *14*, 80.
[33] T.-Y. Lin, H. Masunaga, R. Sato, A. D. Malay, K. Toyooka, T. Hikima, K. Numata, *Biomacromolecules* **2017**, *18*, 1350.
[34] A. D. Malay, T. Suzuki, T. Katashima, N. Kono, K. Arakawa, K. Numata, *Sci. Adv.* **2020**, *6*, eabb6030.
[35] G. Askarieh, M. Hedhammar, K. Nordling, A. Saenz, C. Casals, A. Rising, J. Johansson, S. D. Knight, *Nature* **2010**, *465*, 236.
[36] L. R. Parent, D. Onofrei, D. Xu, D. Stengel, J. D. Roehling, J. B. Addison, C. Forman, S. A. Amin, B. R. Cherry, J. L. Yarger, N. C. Gianneschi, G. P. Holland, *Proc. Natl. Acad. Sci. USA* **2018**, *115*, 11507.
[37] Z. Lin, W. Huang, J. Zhang, J. S. Fan, D. Yang, *Proc. Natl. Acad. Sci. USA* **2009**, *106*, 8906.
[38] D. Huemmerich, C. W. Helsen, S. Quedzuweit, J. Oschmann, R. Rudolph, T. Scheibel, *Biochemistry* **2004**, *43*, 13604.
[39] J. Bauer, D. Schaal, L. Eisoldt, K. Schweimer, S. Schwarzinger, T. Scheibel, *Sci. Rep.* **2016**, *6*, 34442.
[40] J. Bauer, T. Scheibel, *Biomacromolecules* **2017**, *18*, 2521.
[41] S. Rammensee, U. Slotta, T. Scheibel, A. Bausch, *Proc. Natl Acad. Sci. USA* **2008**, *105*, 6590.
[42] U. Slotta, S. Hess, K. Spieß, T. Stromer, L. Serpell, T. Scheibel, *Macromol. Biosci.* **2007**, *7*, 183.
[43] A. Heidebrecht, L. Eisoldt, J. Diehl, A. Schmidt, M. Geffers, G. Lang, T. Scheibel, *Adv. Mater.* **2015**, *27*, 2189.
[44] M. E. Kinahan, E. Filippidi, S. Köster, X. Hu, H. M. Evans, T. Pfohl, D. L. Kaplan, J. Wong, *Biomacromolecules* **2011**, *12*, 1504.
[45] B. Madsen, Z. Z. Shao, F. Vollrath, *Int. J. Biol. Macromol.* **1999**, *24*, 301.
[46] J. Garrote, V. Ruiz, O. P. Troncoso, F. G. Torres, M. Arnedo, M. Elices, G. V. Guinea, J. Pérez-Rigueiro, *J. Mech. Behav. Biomed. Mater.* **2020**, *111*, 104023.
[47] A. A. Komar, *Trends Biochem. Sci.* **2009**, *34*, 16.
[48] F. U. Hartl, M. Hayer-Hartl, *Nat. Struct. Mol. Biol.* **2009**, *16*, 574.
[49] H. Yamaguchi, M. Miyazaki, *Biomolecules* **2014**, *4*, 235.
[50] D. P. Knight, F. Vollrath, *Naturwissenschaften* **2001**, *88*, 179.
[51] Y. Aoyanagi, K. Okumura, *Phys. Rev. Lett.* **2010**, *104*, 038102.
[52] U. K. Slotta, S. Rammensee, S. Gorb, T. Scheibel, *Angew. Chem., Int. Ed.* **2008**, *47*, 4592.